EurJIC
European Journal of Inorganic Chemistry

Full Papers
doi.org/10.1002/ejic.202100653

Chemistry Europe
European Chemical Societies Publishing

Versatile Heteroleptic Cu(I) Complexes Based on Quino(xa)-line-Triazole Ligands: from Visible-Light Absorption and Cooperativity to Luminescence and Photoredox Catalysis

Cecilia Bruschi,[a] Xin Gui,[b] Nasrin Salaeh-arae,[a] Tobia Barchi,[a] Olaf Fuhr,[c, d] Sergei Lebedkin,[c] Wim Klopper,[b] and Claudia Bizzarri*[a]

Four new heteroleptic Cu(I) complexes based on 1, 2, 3-triazolyl-quinoline or quinoxaline and a chelating diphosphine were prepared and fully characterised. The mononuclear derivatives absorb in the visible region, up to 600 nm, while the dinuclear complex has a long-tail absorption up to 800 nm, showing an additional electronic state corroborated by theoretical calculations. Although a methylene group between the triazole and the quino(xa)line moiety increases the bite angle and decreases the luminescence in solution, all complexes emit brightly in the solid-state. Their redox properties in the excited state were determined, proving their ability in serving as photoredox catalysts in atom transfer radical addition successfully.

Introduction

Nowadays, the need for clean energy is increasing in the face of an economy that cannot rely on fossil fuels anymore, a limited and non-renewable resource responsible for global damages such as the greenhouse effect. For this reason, many efforts are made for finding new alternative energy systems.[1] Among them, the cleanest and the most easily accessible one is sunlight. Nature can exploit and store this source by converting water and CO_2 into organic compounds such as glucose. Many strategies focus on developing coordination metal complexes to increase sustainability in solar energy conversion[2] and optoelectronic applications.[3] The majority of these transition metal complexes are based on expensive ruthenium, iridium or other rare metals, which are remarkably well-performing, but cannot be considered sustainable in the long term and for widespread use. Therefore, envisioning a global use of such new technologies, we need to shift our attention to other metals that are earth-abundant.[4] Copper is one of the most promising alternatives.[5] This earth-abundant metal has a d^{10} electronic configuration in its oxidative state +1. Non-radiative metal-centred (MC) transitions are consequently forbidden, while Cu(I) complexes exhibit metal-to-ligand charge-transfer (MLCT) transitions, often absorbing at low energy, in the visible region. Since the late 1970s, thanks to the work of McMillin on the room temperature luminescent Cu(I)-bis(1, 10-phenanthrolines),[6] these complexes have attracted the interest of many researchers and have been exploited in different application fields, such as optoelectronics,[7] photovoltaics[8] or photoredox catalysis.[9] Although the development of Cu(I) coordination complexes has started over forty years, they have a vast potential that is still uncovered. They have much shorter excited state lifetimes than Ru(II) or Ir(III) complexes. Heteroleptic Cu(I) complexes made of diimine (NN) and chelating phosphine (PP) with bulky substituents are appealing. Their sterical hindrance is known to reduce the possible Jahn-Teller distortion that affects Cu(I) complexes in their excited state,[10] avoiding possible non-radiative pathways responsible for low emission quantum yield and short-living lifetime. Our scientific target is to develop new Cu(I) complexes that can absorb visible light and find applications as photosensitisers and photoredox catalysts. With this in mind, we look for alternative ligands that can replace the ubiquitous 1, 10-phenanthroline. Thus, in this work, new copper complexes have been synthesised with quino(xa)line-based ligands, expecting an increased absorbance towards long wavelengths (>400 nm). The synthesis of these ligands is straightforward and does not need the use of Pd catalysts as in our previously reported ligands.[11] Furthermore, the quinoxaline heterocycle allows the coordination of a second Cu(I) nucleus, so that a dinuclear complex could be obtained

[a] C. Bruschi, N. Salaeh-arae, T. Barchi, Dr. C. Bizzarri
Institute of Organic Chemistry,
Karlsruhe Institute of Technology
Fritz-Haber-Weg 6,
76137 Karlsruhe, Germany
E-mail: bizzarri@kit.edu
https://www.ioc.kit.edu/bizzarri/english/index.php
[b] Dr. X. Gui, Prof. Dr. W. Klopper
Institute of Physical Chemistry–Theoretical Chemistry
Karlsruhe Institute of Technology (KIT),
Fritz-Haber-Weg 2, 76131 Karlsruhe, Germany
[c] Dr. O. Fuhr, Dr. S. Lebedkin
Institute of Nanotechnology
Karlsruhe Institute of Technology
Hermann-von-Helmholtz Platz 1, 76344Eggenstein-Leopoldshafen, Germany
[d] Dr. O. Fuhr
Karlsruhe Nano MicroFacility (KNMF)
Karlsruhe Institute of Technology
Hermann-von Helmholtz-Platz 1, 76344Eggenstein-Leopoldshafen, Germany

Supporting information for this article is available on the WWW under https://doi.org/10.1002/ejic.202100653

and the cooperativity between these two metal centres was investigated. The chelating phosphine was the bulky bis [(2-diphenylphosphino)phenyl] ether (DPEPhos) for all complexes reported herein. Full electrochemical and photophysical characterisations were performed and their results are supported by theoretical calculations. Finally, these complexes were tested as photoredox catalysts in the atom transfer radical addition (ATRA).[12]

Results and Discussion

Synthesis and X-Ray structures

The diimine ligands presented herein are shown in Scheme 1 together with the respective synthetic steps. These ligands possess the same chelating binding mode: dative bonds from the N atom in position 2 of the 1, 2, 3-triazole and from the N atom in position 1′ of the quinoxalyl (for ligand **5**, **7** and **8**) or quinolyl (for ligand **6**) substituent. They can be synthesised in few steps, without the need of expensive catalysts or harsh conditions. The first step is the synthesis of brominated derivatives of quino(xa)lines. The monobrominated (**9**) and its corresponding dibrominated (**12**) precursors were obtained with high yield through a condensation reaction involving ammonium chloride as catalyst.[13] This reaction was fast (ca. 30 min) and showed an evident stepwise change of colours, from yellow to red and finally to greyish. Differently, the monobrominated precursor **10** was obtained with a modified procedure[14] of a radical bromination reaction, using N-bromosuccinimide as bromine donor and benzoylperoxide as initiator, directly on quinaldine (2-methyl-quinoline). The monobrominated precursor **11** was synthesised adopting both procedures used for other ligands, namely, the condensation reaction followed by the radical bromination. Then, all the bromoderivatives underwent a nucleophile substitution by sodium azide and, in a one-pot reaction, cyclisation with ethynylbenzene *via* a Cu alkyne-azide cycloaddition (CuAAC).[15] For the dichelating ligand **12** a double number of equivalents of NaN_3 and ethynylbenzene was necessary.

The so-obtained ligands needed no further purification and were used for the synthesis of Cu(I) complexes. As known from literature,[16] heteroleptic Cu(I) complexes are formed upon addition of the diimine ligands to a solution of a Cu(I) precursor ($Cu(CH_3CN)_4BF_4$) and a chelating diphosphine (DPEPhos) at room temperature, under inert atmosphere and in dry solvent (dichloromethane, DCM) (see Scheme 1, right side). The mononuclear complexes **1–3** and the dinuclear complex **4** were isolated after removing the solvent under reduced pressure.

The mononuclear complexes formed good quality crystals by slow diffusion of cyclohexane, in which the complexes are not soluble, into their concentrated solutions in dichloromethane. Although we purified complex **4** *via* the same method, the crystals obtained were not good for X-ray diffraction. The X-ray crystal structures of **1–3** are shown in Figure 1. All structures belong to the triclinic system with the P1 space group. The three compounds show similar distances between the metal center and the coordinative nitrogen atoms, with a smaller length between Cu and the triazole (**1**: 2.087 Å, **2**: 2.095 Å, **3**: 2.059 Å) than between Cu and the quino(xa)line (**1**: 2.129 Å, **2**: 2.117 Å, **3**: 2.139 Å). The distances between Cu and the two P atoms also show similarity (**1**: 2.249 Å, **2**: 2.299 Å, **3**: 2.273 Å for Cu-P_1 and **1**: 2.311 Å, **2**: 2.255 Å, **3**: 2.263 Å for Cu-P_2). Moreover, the three complexes show similar angles N_2-Cu-N_4 (**1**: 91.1°, **2**: 89.79°, **3**: 90.6°) and P_1-Cu-P_2 (**1**: 110.59°, **2**: 111.72°, **3**: 113.37°). The bite angles values suggest a pseudo-tetrahedral geometry for all described compounds. Complex **1** presents a weak interaction (Figure S9.1) between the phenyl group of the triazole (at position 4) and a phenyl group bound to P_2 with an angle between the two rings planes of 11.80° and a distance between the two rings centroids of 4.122 Å. Complex **2** shows a weaker interaction involving the same units (Fig-

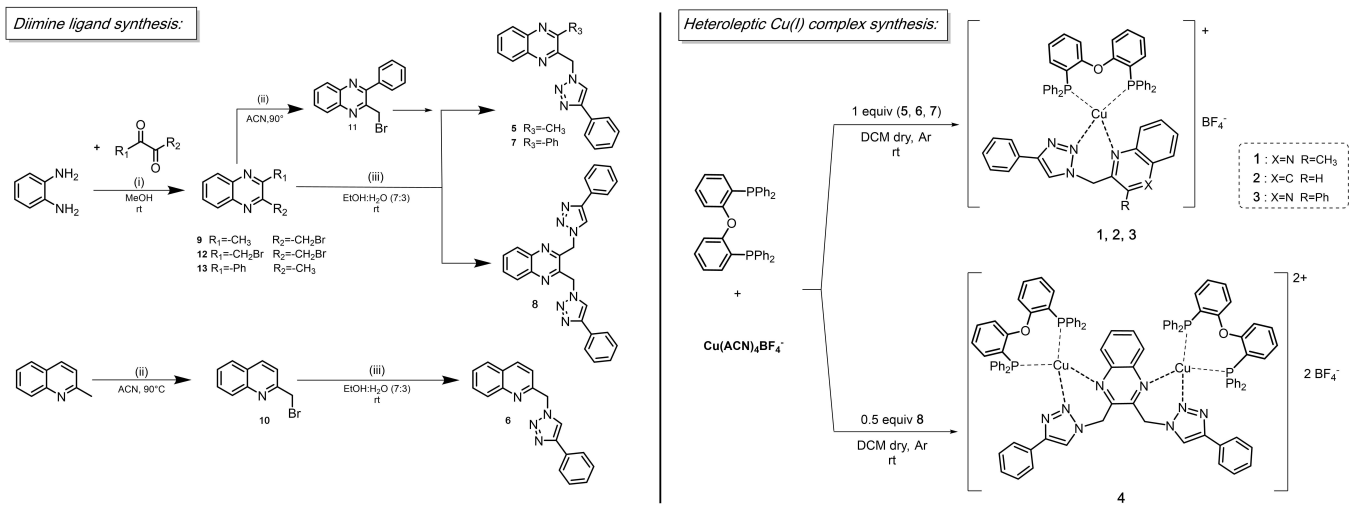

Scheme 1. (Left) Synthetic procedures for the monochelating ligands **5, 6, 7** and dichelating ligand **8**. (i) NH_4Cl; (ii) NBS; benzoylperoxide; (iii) NaN_3; ethynylbenzene; $CuSO_4 \cdot 5H_2O$; sodium ascorbate; Na_2CO_3. (Right) Synthetic procedures for the mononuclear complexes **1**, **2**, **3** and the dinuclear complex **4**.

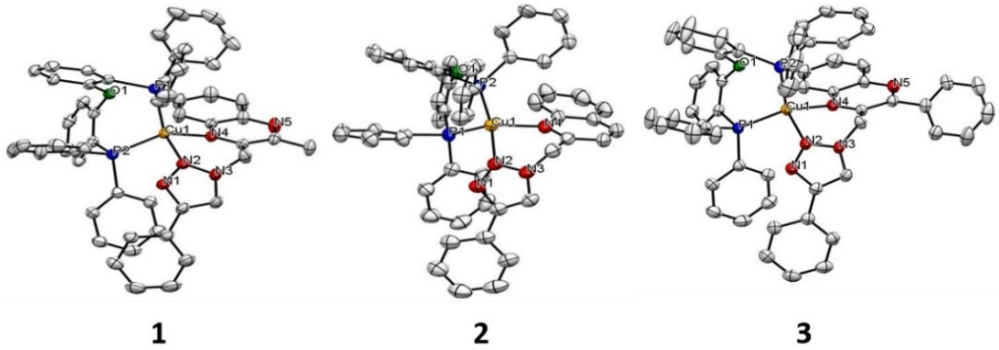

Figure 1. ORTEP drawings of molecular structures of **1**–**3** in the solid state.

ure S9.2, angle between the two planes: 31.44°, distance between the two centroids: 4.580 Å). Differently from the two previous cases, complex **3** has a π-π stacking interaction between one phenyl group bound to P_2 of the DPEPhos and the six-member ring containing the heteroatoms of the quinoxaline moiety of the diimine ligand (see rings E′ and A in Figure S9.3, angle between the two planes: 6.35°, distance between the two centroids: 3.595 Å). Indeed, in complex **3**, the phenyl group of the triazole is interacting not with the phenyl group of the DPEPhos, as in complexes **1** and **2**, but with the phenyl group of the ligand **7** (in position 3′ of the quinoxaline moiety) of the next Cu(I) complex (see G and C rings in Figure S9.5, angle between the two planes: 17.68°, distance between the two centroids: 3.818 Å). Complex **3** is the only complex in this study showing such packing in the solid state.

All four new complexes have a good stability in dichloromethane solvent. Indeed, for each complex the ^{1}H-NMR spectra in CD_2Cl_2 remained identical even after a week (Figures S3.1–S3.4). On the contrary, these compounds are not stable in coordinative polar solvents such as acetonitrile (ACN), methanol, or *N*, *N*-dimethylformamide (DMF). This instability is attributed to decoordination. In fact, the ^{1}H-NMR spectra of the NN ligands and their corresponding complexes are superimposable in ACN, excluding the extra peaks due to DPEPhos in the complex solution (Figures S3.9–S3.16). This lability is correlated to the increased flexibility of NN, due to the presence of the methylene spacer between the quino(xa)line and triazole units, affecting the easiness of ligand exchange. Therefore, a comparison was done for the bond lengths and bite angles between complexes **1**–**4** and previously published Cu-complexes with a related structure $\mathbf{R_1}$[11b] and $\mathbf{R_2}$[11a] (*cf.* Figure 2). In the latter the methylene spacer is absent and they are stable in coordinative polar solvents. Although complexes **1**–**3** show negligible difference in bond lengths ($\Delta < 0.06$ Å), more significant differences are associated with the NN bite angles N_2-Cu–N_4 (ca. 10°) in respect to $\mathbf{R_1}$[11b] and $\mathbf{R_2}$[11a] (Table 1).

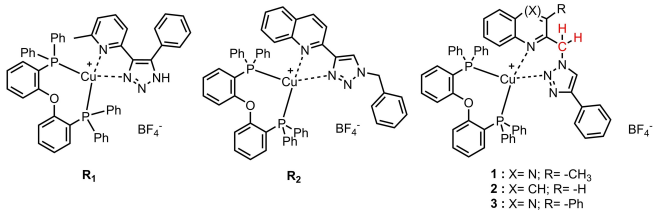

Figure 2. Structures of copper(I) complexes $\mathbf{R_1}$[11b] (left) and $\mathbf{R_2}$[11a] (middle) in comparison to **1**–**3** (right).

Table 1. Selected bond lengths and bond angles for **1**, **2**, **3** and $\mathbf{R_1}$[11b] and $\mathbf{R_2}$.[11a]

	Cu-N_2 Bond length [Å]	Cu-N_4 Bond length [Å]	Cu-P_1 Bond length [Å]	Cu-P_2 Bond length [Å]	N_2-Cu-N_4 Bond angle [°]	P_1-Cu-P_2 Bond angle [°]
1	2.087	2.129	2.249	2.311	91.1	110.59
2	2.095	2.117	2.299	2.255	89.79	111.72
3	2.059	2.139	2.273	2.263	90.6	113.37
$\mathbf{R_1}$[11b]	2.038	2.095	2.217	2.274	79.93	114.59
$\mathbf{R_2}$[11a]	2.069	2.093	2.249	2.249	79.8	116.21

Photophysical characterisation

UV-Vis absorption spectra were recorded for compounds **1**–**4** (Figure 3) and their corresponding ligands **5**–**8** (Figure S5.1) in DCM solutions. The absorption bands in the UV region below 350 nm are dominated by spin allowed transitions centred on the diimine ligands and on the DPEPhos.

The highest absorption peak at ca. 240 nm is attributed to the NN ligands, it has a molar absorption coefficient $\varepsilon = (4\text{–}7)\cdot 10^4\ M^{-1}cm^{-1}$ in **5**–**8** and $\varepsilon = (6\text{–}11)\cdot 10^4\ M^{-1}cm^{-1}$ in **1**–**4**. The absorption at around 280 nm is nearly absent in the NN ligands spectra and, for this reason, can be assigned to a ligand centred transition ^{1}LC on the phosphine ligands. At ca. 320 nm, the absorption can be assigned to a ^{1}LC transition on the quin(ox)aline moiety, since the spectra of the NN ligands also show a similar feature. As a further proof, this value is nearly equal for the monochelating ligand **5** and its corresponding dichelating ligand **8**, in which only one quinoxaline unit is present. Finally, the absorption spectra of the complexes show a low intensity

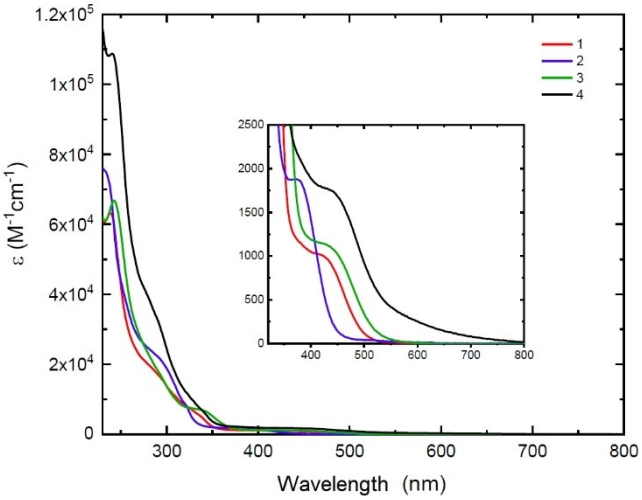

Figure 3. Absorption spectra recorded for complexes **1**, **2**, **3**, **4** in dichloromethane solutions (Inset: zoom-in of the near-UV-vis region).

band starting from the near-UV and extending into the visible region (see insert in Figure 3), which can be assigned to the population of a metal to ligand charge transfer state, ^{1}MLCT. In particular, this MLCT is a transition that goes from the metal core to the quinoxaline unit for complexes **1**, **3** and **4**, and to the quinoline unit for complex **2**. This attribution is corroborated by the theoretical calculations (*vide infra*). The presence of one more electron-donating N atom in the quinoxaline mojety causes a bathochromic shift of the MLCT of **1** (λ_{abs}: 425 nm) in respect to **2** (λ_{abs}: 376 nm), which shows basically the same absorption of the quinoline-based complex $\mathbf{R_2}$.[11a] Complex **3** has a larger bathochromic shift at ca. 435 nm. This is due to the presence of the phenyl substituent in **3** compared to the methyl substituent in complex **1**.

Interestingly, in the absorption spectrum of the dinuclear complex **4**, the ^{1}MLCT transition shows a red shift (at 440 nm), compared to its corresponding mononuclear complex **1**, and a weak new band, centred at around 600 nm. These results were confirmed by theoretical calculations and could be related to a cooperative effect between the two metal centres. To the best of our knowledge, this is one of the few cases of heteroleptic copper(I) complexes[18] where two copper centres share the same NN ligand and consequently the same lowest unoccupied energy level, (LUMO), centred in this case on the quinoxaline unit. Differently, most of the published dinuclear copper complexes show two separated coordinated copper units, each with its own LUMO level, communicating through a bridge unit, e.g. amine based ligand[11a,16] or phosphine based ligand.[19,17,20]

The stability of all complexes in dichloromethane, as already verified by ^{1}H-NMR spectra, was checked with absorbance spectra recorded at different times. The absorbance spectra of all complexes do not show any change after a week and they do not show any new peak (Figures S3.5–S3.8), which could have been attributed to the absorption of an *in situ* formed homoleptic complex $[Cu(NN)_2]^+$.

The emission spectra for **1**–**3** were recorded under inert atmosphere (Ar) in dichloromethane at room temperature (Figure 4). While no emission of the dinuclear complex **4** was detectable at room temperature, the spectra of **1**–**3** present broad and structureless profile, as it is typical for MLCT transition. Moreover, the photoluminescence (PL) is quenched in air-equilibrated solutions, suggesting an involvement of the triplet excited state, undergoing a triplet-triplet annihilation process with molecular oxygen.

The emission maxima are observed at ca. 741, 643 and 670 nm for **1**, **2** and **3**, respectively. Interestingly, the emission of **3** is blue-shifted compared to **1**, despite its red-shifted ^{1}MLCT absorption band. This result suggests that a lower stabilisation of the excited state occurs for **3** in respect to **1**, since a higher stericall hindrance is caused by the phenyl substituent in position 3′ of the quinoxaline moiety in complex **3**, in comparison to the methyl group in complex **1**. This may have a significant role in contrasting the Jahn-Teller effect,[21] typical for Cu(I) complexes in their excited state.[22] Emission quantum yields are up to 1% in solution at room temperature for the three emitting complexes. The excited-state lifetimes of complexes **1** (49 ns) and of **3** (43 ns) are one order of magnitude lower compared to the lifetime of **2** (528 ns). However, since the quantum yield of **3** is only about three times lower compared to the one of **2**, this implies that both the radiative (k_r) and non-radiative constants (k_{nr}) of the quinoxaline based complex **3** are higher compared to the quinoline based complex **2**. The PL lifetimes of **1**–**3** are short when compared to the complex $\mathbf{R_2}$[11a] ($\tau = 2.25$ µs). This is especially surprising for complex **2**, which shows almost the same emission as $\mathbf{R_2}$.[11a] Therefore, this is a further evidence that the methylene spacer between the quinoline and triazole units is responsible for more efficient non-radiative deactivation pathways in solution for **2**, as compared to $\mathbf{R_2}$.[11a] Excitation spectra of **1**–**3** complexes

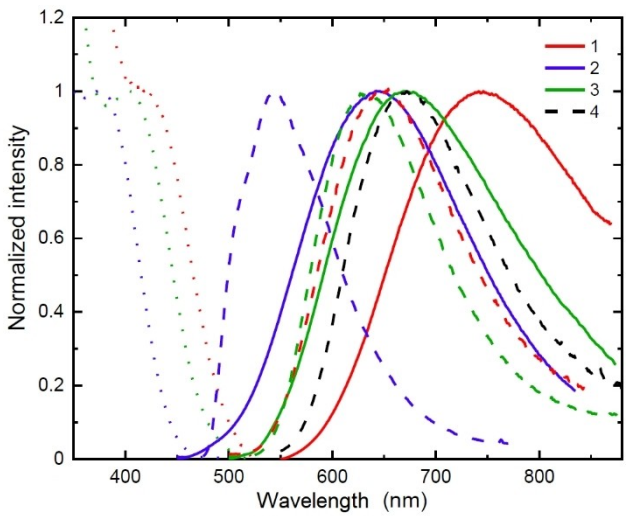

Figure 4. Emission (solid curves) and excitation (dotted curves) spectra of **1**, **2**, **3** recorded at room temperature (298 K) in Ar-saturated dichloromethane solutions. Dashed curves: emission spectra of **1**–**4** recorded in a dichloromethane rigid matrix at 77 K.

were also recorded and they fit nicely with the corresponding absorption spectra.

Emission spectra of all complexes were recorded also in a dichloromethane rigid matrix at 77 K (dashed curves, Figure 4). The mononuclear complexes show a maximum emission that has a hypsochromic shift compared to the emission spectra recorded at room temperature, attributed to a rigidochromic effect, confirming the contribution of a MLCT to the emissive state at room temperature. The emission spectra of the mononuclear complex **1**, **3** and of the dinulcear complex **4** are broad and structureless even at 77 K. On the other hand, the emission profile of **2** suggests a more structured shape, which indeed is manifested in solid state (Figure 5). The emission maxima of **1**–**3** at 77 K maintain the same order as at room temperature (λ_{max}: 649 nm, 543 nm, 632 nm for **1**, **2** and **3** respectively). At 77 K even the dinuclear complex **4** emits (λ_{max}: 671 nm). Comparing its emission to that of the corresponding mononuclear complex **1**, the maximum wavelength is red-shifted, confirming the presence of an additional excited state. All photophysical properties are summarised in Table 2.

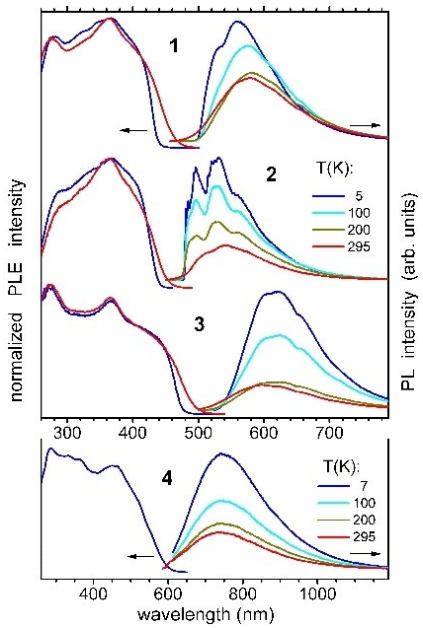

Figure 5. Emission (PL) and excitation (PLE) spectra of solid (polycrystalline) complexes **1**–**4** in the temperature range of 5–295 K. The spectra were excited/ recorded at 350/560, 350/540, 400/620 nm and 450/800 nm, respectively.

In contrast to their weak PL in solution, **1**–**3** display bright emission in the solid-state with quantum yields of 43, 31 and 16 %, respectively, determined at room temperature using an integrating sphere and excitation at 350 nm. In line with the observation of practically absent PL of the dinuclear complex **4** in solution, only very weak phosphorescence at ca. 737 nm was detected for the solid compound (Figure 5). Its efficiency was estimated as 0.38 % at room temperature. By cooling **1**–**4** down to 5 K, the PL efficiency approaches, respectively, 70, 95, 70 and 1.2 %, as estimated from the temperature-dependence emission spectra (Figure 5). Such high efficiency may be attributed to rigid molecular structures in the solid state and the absence of (co-crystallized) solvent molecules in the coordination sphere. Another distinct feature of the solid-state emission of **1**–**3** is its significant blue shift compared to the DCM solutions, with the maxima at about 580, 540 and 600 nm at 295 K. The onsets of absorption in the excitation (PLE) spectra correspond, however, to those in solution. Noteworthy, the emission spectra of **3** is red-shifted compared to the one of **1**, while at room temperature their emission maxima are inverted. This behavior could be correlated to the packing observed in the X-ray crystal structure of **3**.

Note that the solid-state absorption/ PLE spectra are expected to overemphasise the intensity of weak MLCT bands due to high optical thickness and non-validity of the Beer-Lambert law for polycrystalline sample preparations such as used in this work. The PL decay occurs for solid complexes **1**–**3** on the time scale of a few milliseconds – hundreds of microseconds at low temperatures and moderately accelerates at 295 K, roughly correlating with the decrease of the PL intensity (Figure S5.3). Such long lifetimes clearly indicate that the emission is phosphorescence, supporting the above conclusions derived from the PL properties of **1**–**3** in solution. At

Table 2. Photophysical properties of the complexes **1**–**4** in solution (DCM) and in solid state.

Sample	Solution 298 K λ_{abs} [nm]	λ_{em} [nm]	PLQY[a]	τ[b] [ns]	k_r [s^{-1}]	k_{nr} (s^{-1})	Solid state 77 K λ_{em} [nm]	298 K λ_{em} [nm]	PLQY[c]	τ[d] [ms]	5 K λ_{em} [nm]	PLQY[c]	τ[d] [ms]
1	425	741	< 0.001	49	/	/	649	580	0.43	0.20 (65 %) 0.055 (35 %)	557	0.70	1.43 (55 %) 0.40 (45 %)
2	376	643	0.01	528	$1.89 \cdot 10^4$	$1.88 \cdot 10^6$	543	540	0.31	0.36 (72 %) 0.072 (28 %)	496, 530, 560	0.95	1.63 (72 %) 0.52 (28 %)
3	435	670	0.004	43	$9.30 \cdot 10^4$	$2.32 \cdot 10^7$	632	600	0.16	0.026 (52 %) 0.0093 (48 %)	621	0.70	0.33 (61 %) 0.14 (39 %)
4	440, 600	n.d.	n.d.	n.d.	/	/	672	737	0.0038	$45 \cdot 10^{-6}$(65 %) $250 \cdot 10^{-6}$(35 %)	742	0.012[e]	$0.81 \cdot 10^{-3}$(70 %) $6.9 \cdot 10^{-3}$(30 %)[e]

[a] PLQY values in the solution were estimated using $Ru(bpy)_3Cl_2$ in aerated water solution as reference (PLQY = 0.040).[23,24] [b] Lifetimes in solution a room temperature were recorded with a time correlated single photon counting and with Nanoled as excitation source (λ_{exc} = 368 nm). [c] PLQY values in the solid state were measured at 298 K using an integrating sphere and estimated at 5 K from the temperature-dependent emission spectra. [d] Lifetimes in the solid state were recorded by connecting a photomultiplier to a fast oscilloscope and using a nitrogen laser (~2 nsec, ~5 μJ per pulse) for pulsed excitation at 337 nm. Indicated lifetimes with relative weights in percent correspond to biexponential decay traces. [e] This value was measured at 7 K.

low temperatures, in particular below ~100 K, complex **2** shows vibronically well-structured emission spectra, whereas the emission of **1** and **3** remains nearly structureless (Figure 5).

This difference might relate to the different patterns of π-π stacking interaction in solid **1**–**3** (with the less pronounced one in case of **2**), as discussed above. Complex **3** is the only one showing a bathochromic shift at lower temperatures, indicating for this complex the possibility of a TADF behaviour.[25] Non-radiative relaxation is thus strongly dominating in **4**. Correspondingly, the PL decay is relatively fast, with an effective lifetime of ca. 4 μs at 7 K (Figure S5.3).

Electrochemical characterisation

Cyclic voltammetry (CV) of compounds **1**–**4** was performed in Ar-saturated DCM solutions using tetrabutylammonium hexafluorophosphate ($TBAPF_6$) as supporting electrolyte. All the CV herein presented are reported vs. ferrocene (Fc/Fc^+), used as an internal standard[26] (Figure 6). For comparison, the CV of the diimine ligands **5**–**8** was measured (Figures S6.1–S6.4). Because of reduced solubility in DCM of ligands **6** and **8**, their CV were measured in DMF. All complexes show an irreversible oxidation process that is assigned to the Cu^I/Cu^{II} oxidation. These oxidation potentials are at ca. 0.95 V for **1**, **3** and dinuclear complex **4**, while the oxidation of **2** occurs ca. 150 mV earlier and it is quasi reversible. Moreover, when observing the current associated with the oxidation process of **4**, this is ca. the double of the current associated with the mononuclear complexes, equal concentrations used. This is an indication that the two Cu(I) centres oxidise simultaneously under these conditions. Compounds **1** and **2** show irreversible reduction at ca. −2.3 V, while **3** displays additional, also irreversible, reduction processes at −2.17 V and −2.50 V. The dinuclear complex **4** shows three reduction processes, which occur at higher potential compared to the corresponding mononuclear complex **1** (-1.30 V, −1.73 V, −2.0 V). All the reduction processes could be attributed to the diimine ligands, although the reduction processes in **1**–**4** occur at ca. 200 mV higher potential than in their corresponding ligands.

In order to use these compounds in photoredox catalysis, it is important to evaluate their redox potentials in the excited (triplet) state E_{ox} (PS^{*+}) and E_{red} (PS^{*-}). These parameters were calculated by estimating the E_{00} value, which is the energy difference between the zero vibrational levels of the excited and ground states.[27] The estimation adopted equations found in literature.[28,29] The reduction and oxidation potentials of complexes **1**–**4** in their ground and excited states are listed in Table 3.

Quantum chemical calculations

The ground-state (S_0) geometries of the mononuclear complexes **1**–**3** (Table 4) were optimised at PBE0-D3(BJ) level of theory starting from the obtained X-ray diffraction structures. The S_0 geometry of the dinuclear complex **4** was built and optimised based on the structure of **1** (Table 4).

To further investigate the photophysical properties of the heteroleptic copper(I) complexes, quantum chemical calculations utilising the *GW* approximation and Bethe–Salpeter equation (*GW*/BSE) were performed at both one component (1c, scalar-relativistic) and quasirelativistic two-component (**2c**, including spin-orbit coupling) levels.

At the optimised S_0 geometry, the calculated absorption spectra (Figure S7.1) agree well with the experimental results. The MLCT absorption bands are occurring with relative maxima

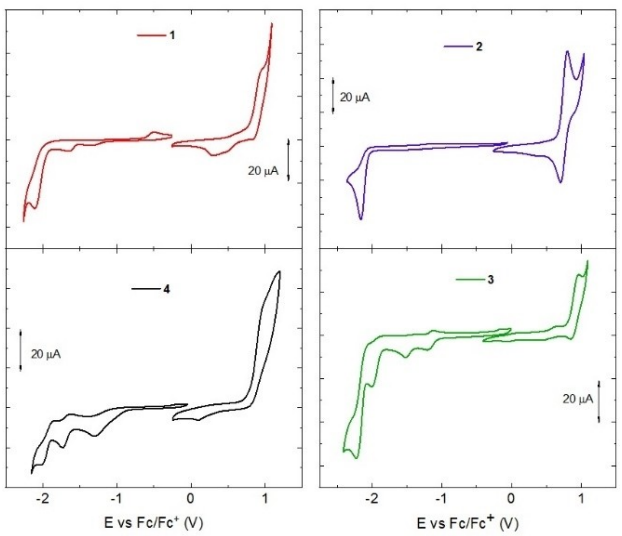

Figure 6. CV of **1**–**4** recorded at room temperature in Ar-saturated dichloromethane solutions (0.2 M $TBAPF_6$) at scan rate 100 mV s^{-1} and reported versus Fc/Fc^+.

Table 3. Reduction and oxidation potentials of copper complexes **1**–**4** in DCM.[a]

Sample	E_{ox} [V]	E_{red} [V]	E_{ox}* [V][b]	E_{red}* [V][b]
1	0.88	−2.30	−1.37	−0.05
2	0.75	−2.40	−2.27	0.62
3	0.90	−2.17, −2.50	−1.99	0.72
4	0.89	−1.30, −1.73, −2.00	n.d.	n.d.

[a] Obtained by cyclic voltammetry, at scan rate 100 mV s^{-1}, using ferrocene as internal reference. [b] Redox values for the excited states were calculated using the following equations: $E_{ox}^* = E_{ox} - E_{00}$; $E_{red}^* = E_{red} + E_{00}$ where the E_{00} values were estimated (2.25 V for **1**, 3.02 V for **2**, 2.89 V for **3**) as described in literature.[28,29]

Table 4. Calculated bond lengths and bond angles for **1**–**4**.

	Bond length [Å] Cu-N_2	Bond lenght [Å] Cu-N_4	Bond length [Å] Cu-P_1	Bond length [Å] Cu-P_2	Bond angle [deg] N_2-Cu-N_4	Bond angle [deg] P_1-Cu-P_2
1	2.130	2.135	2.257	2.316	93.6	114.4
2	2.132	2.126	2.256	2.312	92.9	114.3
3	2.105	2.126	2.254	2.314	93.4	114.4
4	2.117	2.142	2.256	2.316	90.0	115.8

at 438 nm for **1**, 397 nm for **2**, 447 nm for **3**, 431 and 645 nm for **4**, which fit nicely with the experimental values, with a slight red-shifted up to 0.18 eV. A natural transition orbital (NTO) analysis confirms the MLCT character of the transitions in the visible region (Figure S7.2). The first absorption band of all four complexes corresponds to charge transfer from the copper atom to the quinoline/quinoxaline moiety of the diimine ligand, while the triazole moiety is not involved. For complex **2**, less delocalisation of π electrons on the quinoline ring can be seen from the particle NTO compared to the quinoxaline, which leads to higher energy levels of quinoline π orbitals, and hence the absorption is shifted to higher energy. Besides the lowest absorption band at 645 nm, the dinuclear species **4** exhibits one further MLCT transition at 431 nm compared to the monomers (Figure 7). This arises from the electron coupling between the two copper centers.

Photocatalytic ATRA reaction

Once the new complexes reported here were characterised photophysically and electrochemically, their performance as photoredox catalysts was tested. The reaction selected was the atom transfer radical addition (ATRA, Scheme 2). This process, as far as we know, has already been proved in several studies to be successfully catalysed by homoleptic copper complexes[30] but only once by heteroleptic copper complexes.[31] Photocatalytic tests were carried out by irradiating for 20 h with a 420 nm lamp a dichloromethane solution containing styrene and carbon tetrabromide, with a catalytic amount of the heteroleptic copper complexes (5% for **1**–**2** and 1% for **3**). The best performing photoredox catalyst in this work was complex **2** (Table 5).

In fact, when **2** was used, the desired ATRA product was obtained with a high yield of 86% (Table 5, entry 1). Differently, copper complexes **1** and **3** did not show catalytic activity in the above-mentioned conditions, leading to the same low amount of product as obtained for the reaction carried out without the catalyst (entry 4). The product was not observed, when the reaction was performed in the dark. Then, photocatalytic tests were performed in a biphasic system with an aqueous solution of ascorbic acid (1 M), as sacrificial electron donor, for complexes **1**–**3** (1% of photocatalyst). In these conditions, we could obtain an almost three times higher yield compared to the reaction carried out in the absence of the catalyst, although lower than 50% (Table S8.1). The same reaction was repeated, using a higher amount of photocatalyst, 5% for the mononuclear complex **1** and 2.5% for the dinuclear complex **4** . Surprisingly, even though the photophysical and oxidation properties of **4** are less promising for a photocatalytic application as compared to **1**, the product yield is similar in these reaction conditions (ca. 40%). Since the Cu(I) complex **2** was the one giving the best results, it was tested in another ATRA reaction using iodoform (CHI_3) as the organic halide. In this case, the yield obtained was modest (28%). However, it is still the double value of the yield obtained without the catalyst (Table 5, entry 7). Furthermore, complex **2** gave better results under blue light irradiation also in comparsion to the frequently used iridium(III) or ruthenium(II) photoredox catalysts (reported maximum yield of 15%).[30h] The inferior photocatalytic results for copper complexes **1** and **3** in respect to **2** could be explained considering the much lower lifetime and the lower oxidation reduction of the excited state of the former compounds. Both factors play an important role for the efficiency of a photocatalytic reaction.

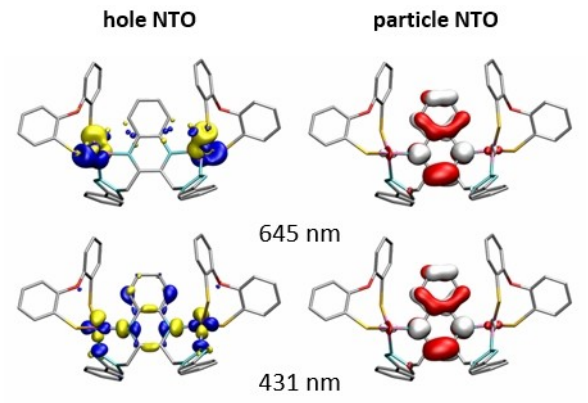

Figure 7. Dominating occupied (blue/yellow) and virtual (red/white) natural transition orbitals (NTOs, iso-value: $\pm 0.04\alpha_0^{-3/2}$) of the MLCT excitation of **4** calculated at PBE0 ev*GW*-BSE/def2-TZVP level. Phenyl groups of DPEPhos and all hydrogen atoms are omitted for clarity.

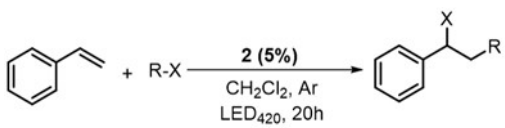

Scheme 2. ATRA reaction with styrene and organic halide (CBr_4 or CHI_3) at 25 °C for 20 h.

Table 5. Visible light induced ATRA reactions with **2** as photoredox catalyst.

Entry	Catalyst	Organic halide	λ [nm]	Yield[a] [%]
1[b]	2	CBr_4	420	86%
2[b]	2	CBr_4	420	80[c]
3[b]	2	CBr_4	no	/
4[b]	no	CBr_4	420	21
5[d]	2	CHI_3	420	28
6[d]	2	CHI_3	no	/
7[d]	no	CHI_3	420	14

[a] The yield was estimated using dodecane anhydrous as internal reference. [b] Styrene (1 equiv), CBr_4 (1 equiv), **2** (5%), irradiation at 420 nm for 20 h in dichloromethane dry (1.5 mL). [c] The yield is calculated for the product isolated by flash chromatography. [d] Styrene (2 equiv), CHI_3 (1 equiv), **2** (5%), irradiation at 420 nm for 20 h in dichloromethane dry (1.5 mL).

Conclusion

We presented three mononuclear and one dinuclear Cu(I) complexes based on derivatives of quino(xa)lyl-1, 2–3-triazole as diimine ligand and DPEPhos as chelating diphosphine. Their electronic and photophysical properties were fully characterised in solution and in solid-state. Thanks to the bis-diimine ligand, the dinuclear complex shows additional electronic states, suggesting a communication between the two metal centres. Although the four complexes show modest or no emission in solution, their luminescence properties in solid-state are promising for optoelectronic applications, with a Φ up to 40% at room temperature. Nevertheless, for photocatalysis, it is not always needed a high luminescent complex in solution. Indeed, we tested their activity as photoredox catalysts in a blue-light driven ATRA reaction with styrene as starting material and tetrabromomethane or iodoform as organic halide. The yields obtained with one mononuclear complex (**2**) are only slightly lower than those reported in the literature for other homoleptic Cu(I) complexes. The promising results of this work motivate further optimisation of the electronic and photophysical properties of Cu(I) complexes, which is a challenge that has to be overcome to pursue a more sustainable chemistry.

Experimental Section

Synthesis

Synthesis of 2-(bromomethyl)-3-methylquinoxaline (9): Bromobutane-2, 3-dione (0.279 g, 1.85 mmol, 1.00 equiv) was dissolved in 5 mL MeOH, followed by ammonium chloride (49 mg, 0.93 mmol, 0.50 equiv) and 1, 2-phenylendiamine (0.200 g, 1.85 mmol, 1.00 equiv). The reaction mixture was stirred at room temperature for 30 minutes. Then water was added and the organic products were extracted with dichloromethane (3 times). The organic phase collected was washed with brine, dried over Na_2SO_4, and filtered. The solvent was removed under vacuum. The product was used without any further purification for the next step, since the ^{1}H-NMR analysis revealed the product was clean. The product was a light brown solid. 328 mg. (Yield:75%) ^{1}H-NMR (400 MHz, $CDCl_3$) δ [ppm] = 8.06–8.00 (m, 2H), 7.77–7.70 (m, 2H), 4.76 (s, 2H), 2.89 (s, 3H). ^{13}C-NMR (126 MHz, $CDCl_3$) δ [ppm] = 153.24 (C_q), 150.98 (C_q), 142.09 (C_q), 140.95 (C_q), 130.58 (+, $C_{Ar}H$), 129.61 (+, $C_{Ar}H$), 129.14 (+, $C_{Ar}H$), 128.53 (+, $C_{Ar}H$), 31.94 (−, CH_2), 22.57 (+, CH_3).

Synthesis of 2-(bromomethyl)quinoline (10): According to a modified procedure,[14] 2-methyl-quinoline (0.500 g, 3.49 mmol, 1.00 equiv) was reacted with N-bromsuccinimide (1.236 g, 6.98 mmol, 2.00 equiv) and benzoylperoxide (0.339 g, 1.39 mmol, 0.40 equiv) in acetonitrile under argon atmosphere. The reaction mixture was left under stirring, at 90 °C for 25 h. Water was afterwards added for the quenching and the product was extracted successively with dichloromethane (3 times), dried over Na_2SO_4, and filtered. The solvent was removed under reduced pressure. The crude product was purified by silica gel chromatographic column using the Cy:EtOA = (95:5) as eluent. 105 mg (Yield: 13%) ^{1}H-NMR (300 MHz, $CDCl_3$) δ [ppm] = 8.20 (t, J = 8.8 Hz, 1H), 8.07 (dq, J = 8.5, 1.0 Hz, 1H), 7.86–7.78 (m, 1H), 7.74 (ddt, J = 8.4, 6.9, 1.5 Hz, 1H), 7.63–7.52 (m, 2H), 4.72 (s, 2H).

Synthesis of 2-methyl-3-phenylquinoxaline (13): 2-methyl-3-phenylquinoxaline was synthesised from phenyl-1, 2-propanedione and 1, 2-phenylendiamine using the same procedure adopted for 2-(bromomethyl)-3-methylchinoxaline (**9**). In this case the crude product was further purified by silica gel chromatographic column using Cy:EtOA = (95:5) as eluent. 2.416 g (Yield: 78%). ^{1}H-NMR (300 MHz, CDCl3) δ [ppm] = 8.17–8.09 (m, 1H), 8.09–8.01 (m, 1H), 7.79–7.69 (m, 2H), 7.69–7.61 (m, 2H), 7.57–7.44 (m, 3H), 2.78 (s, 3H).

Synthesis of 2-(bromomethyl)-3-phenylquinoxaline (11): 2-methyl-3-phenylquinoxaline was reacted with N-bromsuccinimide and benzoylperoxide following the same procedure as used for 2-(bromomethyl)quinoline (**10**) in order to get the desired product **11**. 337 mg (Yield: 30%) ^{1}H-NMR (300 MHz, $CDCl_3$) δ [ppm] = 8.18–8.11 (m, 2H), 7.83–7.74 (m, 4H), 7.59–7.52 (m, 3H), 4.76 (s, 2H).

Synthesis of 2, 3-bis(bromomethyl)quinoxaline (12): 2, 3-bis (bromomethyl)quinoxaline was synthetized using the same procedure adopted for 2-(bromomethyl)-3-methylchinoxaline, using 1, 4-dibromobutane-2, 3-dione as starting material. The product was used without any further purification for the next step, since the ^{1}H-NMR analysis revealed the product was clean. The product was a lightly brown solid. 203 mg (Yield: 97%) ^{1}H-NMR (300 MHz, $CDCl_3$) δ [ppm] = 8.15–8.02 (m, 2H), 7.85–7.76 (m, 2H), 4.93 (s, 4H). 13 C NMR (126 MHz, $CDCl_3$) δ [ppm] = 151.01 (C_q), 141.72 (C_q), 131.12 (+, $C_{Ar}H$), 129.20 (+, $C_{Ar}H$), 30.63 (−, CH_2).

General procedure for the synthesis of the monochelating ligands 5, 6, 7: According to a modified procedure,[32] the monobrominated starting ligand **9–11** (1.00 equiv) was dissolved into a solution of ethanol and water (7:3). Then the other reactants were added in the following order: sodium azide (1.20 equiv), sodium ascorbate (0.562 equiv), copper sulfate pentahydrate (0.204 equiv), sodium carbonate (0.591 equiv), ethynylbenzene (1.00 equiv). Please, be careful and use protective equipment when using NaN_3, as it can be explosive. The reaction mixture was left under stirring at room temperature for two days. A solution of NH_4OH (10%) was subsequently added for the quenching. The organic product was extracted three times with dichloromethane, then it was washed with water and brine, dried over Na_2SO_4 and filtered. Lastly, the solvent was removed under reduced pressure.

5: White powder. 179 mg (Yield: 71%) ^{1}H-NMR (400 MHz, CD_2Cl_2) δ 8.04–8.00 (m, 2H), 7.96 (s, 1H), 7.84–7.80 (m, 2H), 7.75 (dddd, J = 16.6, 8.4, 7.0, 1.7 Hz, 2H), 7.44–7.39 (m, 2H), 7.35–7.30 (m, 1H), 5.93 (s, 2H), 2.81 (s, 3H).^{13}C-NMR (126 MHz, $CDCl_3$) δ [ppm] = 152.78 (C_q), 148.22 (C_q), 142.10 (C_q), 140.75 (C_q), 130.73 (+, $C_{Ar}H$), 130.38 (C_q), 129.67 (+, $C_{Ar}H$), 129.10 (C_q), 128.85 (+, $C_{Ar}H$), 128.58 (C_q), 128.30 (+, $C_{Ar}H$), 125.75 (+, $C_{Ar}H$), 54.06 (−, CH_2), 22.48 (+, CH_3). HRMS *m/z* ($C_{18}H_{15}N_5$): 301.1327 (calc); 301.1326 (found).

6: White powder. 130 mg (Yield: 55%) ^{1}H-NMR (300 MHz, CD_2Cl_2) δ 8.30 (s, 1H), 8.22–8.09 (m, 2H), 7.99 (d, J = 7.8 Hz, 1H), 7.88–7.74 (m, 2H), 7.72–7.56 (m, 2H), 7.33 (d, J = 8.5 Hz, 2H), 7.09 (d, J = 7.7 Hz, 1H), 5.93 (s, 2H). ^{13}C-NMR (126 MHz, $CDCl_3$) δ [ppm] = 154.78 (C_q), 148.58 (C_q), 147.80 (C_q), 137.96 (+, $C_{Ar}H$), 130.58 (C_q), 130.40 (+, $C_{Ar}H$), 129.33 (+, $C_{Ar}H$), 128.97 (+, $C_{Ar}H$), 128.37 (+, $C_{Ar}H$), 127.88 (+, $C_{Ar}H$), 127.73 (C_q), 127.35 (+, $C_{Ar}H$), 125.87 (+, $C_{Ar}H$), 120.34 (+, $C_{Ar}H$), 119.82 (+, $C_{Ar}H$), 56.63 (−, CH_2). HRMS *m/z* ($C_{18}H_{14}N_4$): 286.1218 (calc); 286.1218 (found).

7: Greenish powder. 204 mg (Yield: 46%) ^{1}H NMR (400 MHz, CD_2Cl_2) δ 8.14 (dd, J = 8.2, 1.6 Hz, 1H), 8.11–8.07 (m, 1H), 7.92 (s, 1H), 7.87–7.76 (m, 4H), 7.67 (dd, J = 6.7, 3.0 Hz, 2H), 7.59 (q, J = 3.2, 2.6 Hz, 3H), 7.42 (t, J = 7.5 Hz, 2H), 7.33 (t, J = 7.4 Hz, 1H), 5.92 (s, 2H).^{13}C-NMR (126 MHz, $CDCl_3$) δ [ppm] = 154.15 (C_q), 147.57 (C_q), 141.94 (C_q), 141.20 (C_q), 137.43 (C_q), 131.12 (+, $C_{Ar}H$), 130.77 (C_q), 130.58 (+, $C_{Ar}H$), 129.83 (+, $C_{Ar}H$), 129.51 (+, $C_{Ar}H$), 129.28 (C_q), 129.21 (+, $C_{Ar}H$), 129.18 (+, $C_{Ar}H$), 128.96 (+, $C_{Ar}H$), 128.28 (+, $C_{Ar}H$), 125.87 (+, $C_{Ar}H$), 53.67 (−, CH_2). HRMS *m/z* ($C_{23}H_{17}N_5$): 363.1484 (calc); 363.1483 (found).

These are not the final page numbers! ↗↗

Synthesis of the dichelating ligand 8: According to a modified procedure, the dibrominated starting ligand **12** (0.270 g, 0.88 mmol, 1.00 equiv) was dissolved into a 25 mL solution of ethanol and water (7:3) and 2 mL acetonitrile. Then the other reactants were added in the following order: sodium azide (0.137 g, 2.10 mmol, 2.40 equiv), sodium ascorbate (0.198 g, 1.00 mmol, 1.14 equiv), copper sulfate pentahydrate (0.091 g, 0.37 mmol, 0.42 equiv), sodium carbonate (0.087 g, 1.06 mmol, 1.20 equiv), ethynylbenzene (0.179 mg, 1.75 mmol, 2.00 equiv). Please, be careful and use protective equipment when using NaN_3, as it can be explosive. The reaction mixture was left under stirring for two days. Then a NH_4OH (10%) solution was added for quenching the reaction and the organic product was extracted with dichloromethane (3 times). The organic phase collected was washed with brine, dried over Na_2SO_4, filtered. The product is a brown solid. 203 mg (Yield: 52%) ^{1}H-NMR (400 MHz, CD_2Cl_2) δ 8.08 (dt, J = 7.0, 3.5 Hz, 2H), 8.04 (s, 2H), 7.83 (dd, J = 9.4, 7.2 Hz, 6H), 7.42 (t, J = 7.5 Hz, 4H), 7.33 (t, J = 7.0 Hz, 2H), 6.12 (s, 4H). ^{13}C-NMR (126 MHz, $CDCl_3$) δ [ppm] = 148.47 (C_q), 148.21 (C_q), 141.87 (C_q), 131.48 (+, C_{Ar}H), 130.33 (C_q), 129.36 (+, C_{Ar}H), 129.01 (+, C_{Ar}H), 128.52 (+, C_{Ar}H), 125.91 (+, C_{Ar}H), 120.76 (+, C_{Ar}H), 53.52 (−, CH_2). HRMS *m/z* ($C_{26}H_{21}N_8$) 445.1889 (calc); 445.1888 (found).

General procedure for the synthesis of the mononuclear complexes 1, 2, 3: According to literature,[16] $Cu(ACN)_4BF_4$ (1.00 equiv) and DPEPhos (1.00 equiv) were dissolved in dry dichloromethane in a Schlenk flask under argon atmosphere. After 30 minutes, the desired monochelating ligand **5**–**7** (1.00 equiv) was added. The reaction mixture was left under stirring for four hours. Then the solvent was removed under reduced pressure. The crude product was dissolved in a minimum amount of dichloromethane and crystallized by a slow diffusion of cyclohexane.

1: Yellow powder. 500 mg (Yield: 88%) ^{1}H NMR (400 MHz, CD_2Cl_2) δ 8.54 (s, 1H), 8.05 (d, J = 8.5 Hz, 1H), 7.99 (dd, J = 8.6, 1.3 Hz, 1H), 7.60 (ddd, J = 8.4, 6.9, 1.4 Hz, 1H), 7.47–7.42 (m, 2H), 7.32 (td, J = 7.8, 1.7 Hz, 2H), 7.25 (dtd, J = 6.2, 5.0, 2.0 Hz, 7H), 7.17–6.89 (m, 21H), 6.75 (dtd, J = 8.1, 4.2, 1.6 Hz, 2H), 6.01 (s, 2H), 3.00 (s, 3H). ^{13}C NMR (101 MHz, CD_2Cl_2) δ 157.98, 157.92, 157.86, 154.23, 148.70, 147.80, 140.00, 134.57, 133.85, 133.77, 133.70, 132.47, 131.67, 130.72, 130.63, 130.55, 130.37, 129.82, 129.45, 129.20, 129.16, 129.11, 129.05, 126.24, 125.54, 124.38, 123.84, 120.35, 51.98, 23.42. ^{31}P-NMR (162 MHz, CD_2Cl_2) δ −13.99. HRMS (ESI) 902.2232 (z = 1) ($C_{54}H_{43}Cu_1N_5O_1P_2^+$). Calcd for $C_{54}H_{43}Cu_1N_5O_1P_2^+$ BF_4^-. Elemental analysis: [$C_{54}H_{43}BCu_1F_4N_5O_1P_2$]·CH_2Cl_2: C = 61.44, H = 4.22, N = 6.51 (calc.); C = 61.35, H = 4.15, N = 6.57 (found).

2: Brown powder. 322 mg (Yield: 83%) ^{1}H NMR (400 MHz, CD_2Cl_2) δ 8.51 (s, 1H), 8.47 (d, J = 8.4 Hz, 1H), 8.25 (d, J = 8.6 Hz, 1H), 8.06 (d, J = 8.4 Hz, 1H), 7.85 (dd, J = 8.3, 1.4 Hz, 1H), 7.42–7.23 (m, 9H), 7.23–6.97 (m, 23H), 6.72 (dtd, J = 7.8, 4.0, 1.6 Hz, 2H), 6.66 (s, 1H), 5.94 (s, 2H). ^{13}C NMR (101 MHz, CD_2Cl_2) δ 157.90, 157.85, 157.79, 154.33, 148.40, 147.51, 140.55, 134.47, 133.93, 132.17, 131.36, 131.19, 131.02, 130.31, 130.27, 129.78, 129.49, 128.95, 128.89, 128.85, 128.82, 128.75, 128.30, 128.25, 125.99, 125.48, 125.43, 125.40, 125.38, 125.34, 125.20, 123.60, 123.12, 120.42, 54.90.^{31}P-NMR (162 MHz, CD_2Cl_2) δ −13.96. HRMS (ESI) 887.2124 (z = 1) ($C_{54}H_{42}Cu_1N_4O_1P_2^+$). Calcd for $C_{54}H_{42}Cu_1N_4O_1P_2^+$ BF_4^-. Elemental analysis ($C_{54}H_{42}BCu_1F_4N_4O_1P_2$)·$H_2O$: C = 65.30 H = 4.47, N = 5.64 (calc.); C = 65.75, H = 4.37, N = 5.77 (found).

3: Orange powder. 493 mg (Yield: 92%) ^{1}H NMR (400 MHz, CD_2Cl_2) δ 8.11 (s, 3H), 7.79–7.41 (m, 8H), 7.41–7.20 (m, 11H), 7.20–6.96 (m, 19H), 6.77 (dq, J = 8.0, 4.2 Hz, 2H), 5.86 (s, 2H). ^{13}C NMR (101 MHz, CD_2Cl_2) δ 158.09, 148.71, 134.66, 133.67, 132.71, 132.24, 130.85, 129.52, 129.35, 129.24, 126.38, 125.64, 120.34, 54.24 ^{31}P NMR (162 MHz, CD_2Cl_2) δ −14.51. HRMS (ESI) 964.2390 (z = 1) ($C_{59}H_{45}Cu_1N_5O_1P_2$). Calcd for $C_{59}H_{45}Cu_1N_5O_1P_2^+$ BF_4^-. Elemental analysis ($C_{54}H_{42}BCu_1F_4N_4O_1P_2$)·$H_2O$·$CH_2CL_2$: C = 62.38 H = 4.28, N = 6.06 (calc.); C = 62.68, H = 4.20, N = 6.08 (found).

Synthesis of the dinuclear complex 4: According to literature,[16] $(Cu(CH_3CN)_4)BF_4$ (0.133 g, 0.42 mmol, 2.00 equiv) was reacted with DPEPhos (0.192 g, 0.42 mmol, 2.00 equiv) in 25 mL of dry CH_2Cl_2 at room temperature for 30 min, under argon atmosphere. The desired dichelating ligand **8** (93 mg, 0.21 mmol, 1 equiv) was subsequently added to the reaction mixture that was left under stirring over night. Then the solvent was removed under reduced pressure. The crude product was dissolved in a minimum amount of dichloromethane and precipitated by a slow diffusion of cyclohexane. The product was a red powder. 162 mg. (Yield: 42%). ^{1}H NMR (400 MHz, CD_2Cl_2) δ 8.56 (s, 2H), 7.90–7.82 (m, 2H), 7.49 (dt, J = 7.1, 1.4 Hz, 4H), 7.36–7.06 (m, 52H), 7.01 (t, J = 7.4 Hz, 8H), 6.79–6.71 (m, 4H), 6.26 (s, 4H). ^{13}C NMR (101 MHz, CH_2Cl_2) δ 157.94, 148.89, 147.64, 141.43, 134.68, 133.87, 133.79, 133.71, 132.62, 131.73, 130.86, 130.34, 130.16, 129.98, 129.53, 129.34, 129.28, 129.23, 126.57, 125.56, 124.63, 120.32, 52.30.^{31}P NMR (162 MHz, CD_2Cl_2) δ −14.78. HRMS (ESI) 1733, 37 (z = 1) ($C_{98}H_{76}Cu_2N_8O_2P_4^{2+}$ BF_4^-). Calcd for ($C_{98}H_{76}Cu_2N_8O_2P_4^{2+}$·$2BF_4^-$). Elemental analysis: [$C_{98}H_{76}B_2Cu_2F_8N_8O_2P_4$]·H_2O: C = 63.96, H = 4.27, N = 6.09 (calc.); C = 63.83, H = 4.53, N = 6.28 (found).

Electrochemical and photophysical experimental details are reported in the electronic supplementary information.

Computational details

All quantum-chemical calculations were performed with the TURBOMOLE program package.[33] The resolution-of-the-identity (RI) approximation was used for all two-electron integrals. The equilibrium geometries were optimised at the PBE0-D3(BJ) level of theory,[34] and the electronic excitations were calculated at the CD-ev*GW*(10)/BSE level of theory (eigenvalue-only self-consistent *GW* (ev*GW*)[35] employing contour deformation (CD)[36] for the highest 10 occupied and lowest 10 unoccupied orbitals, followed by the Bethe–Salpeter equation (BSE)[37] approach). For non- and scalar-relativistic one-component (1c) calculations, the def2-TZVP basis set was taken for Cu, P, N and C atoms in triazole and quinoline/quinoxaline moieties, and the def2-SV(P) basis set[38] was taken for the rest of the atoms. For quasirelativistic two-component (**2c**) calculations, the all-electron x2c-TZVPall/SV(P)all-2c basis set[39] was used.

All orbital and auxiliary basis sets were taken from the TURBOMOLE basis-set library.[33] The "Coulomb-fitting" auxiliary basis sets (denoted jbas) were used in the ground-state DFT computations, and the "MP2-fitting" auxiliary basis sets (denoted cbas) were used in the excited-state TDDFT and *GW*/BSE computations. The ground-state density functional theory (DFT) computations were carried out with the modules DSCF and RIDFT, and the self-consistent field convergence criterion scfconv = 8 and DFT grid 4 were used. The geometry optimisation was considered converged when the change in energy and cartesian gradients reached thresholds of 10^{-7} hartree and 10^{-4} hartree/bohr, respectively. The excited-state TDDFT and *GW*/BSE computations were carried out with the ESCF module, and the convergence criterion rpaconv = 6 was used. Furthermore, in ev*GW*, the damping parameter was set to $\eta = 0.001$ hartree in order to achieve rapid convergence. In the CD-ev*GW* computations, 128 grid points were used for the numerical quadrature along the imaginary axis.

Crystallography

Deposition Numbers 2074013 (**1**), 2074015 (**2**), 2074016 (**3**), present the supplementary crystallographic data for the crystals structure

shown in this paper. The joint Cambridge Crystallographic Data Centre and Fachinformationszentrum Karlsruhe Access Structures service supplied these data free of charge. Single-crystal X-ray diffraction data were recorded at low temperature on a STADI VARI diffractometer with monochromated Ga Ka (I = 1.34143 Å) or Mo Kα (λ = 0.71073) radiation. Adopting Olex2,[40] the ShelXT[41] structure solution program using Intrinsic Phasing wad selected for determining the structure and the ShelXL[42] refinement package using Least Squares minimisation was selected for refining the structure. Anisotropic temperature factors for all non-hydrogen atoms were adopted for the refinement; hydrogen atoms were computed on idealised positions.

Photoredox catalysis: The experiments were conducted in a Photoreactor from Luzchem (Model: LZC-ICH2). Blue-LED lamps were used at a wavelength of 420 nm. Photon flux was calculated by $K_3Fe(C_2O_4)_3$ actinometry,[43] and it has a value of 4.13 10^{-8} E s^{-1}, equivalent to 2.48 10^{16} photons/s.

General procedure for ATRA reaction with CBr_4: A solution of styrene (170 μL, 1.5 mmol, 1 equiv), CBr_4 (494 mg, 1.5 mmol, 1 equiv) and of the desired complex **2** (73 mg, 0.075 mmol, 5 %) in 1.5 mL of dry CH_2Cl_2, deaerated by bubbling a stream of nitrogen through it for about 10 minutes, was irradiated with a 420 nm LED for 20 h under stirring, placing the sample at a distance of ca. 3 cm from the light source. Then the solvent was removed under reduced pressure. The yield was estimated from the ^{1}H-NMR analysis using dry dodecane as an internal standard. Quantum yield was calculated considering the total number of photons irradiating the reaction vessel for 20 h, and it is 43 %.

General procedure for ATRA reaction with CHI_3: A solution of styrene (57 μL, 0.5 mmol, 2 equiv), CHI_3 (98 mg, 0.25 mmol, 1 equiv) and of the desired complex **2** (12 mg, 0.0125 mmol, 5 %) in 1.5 mL of dry CH_2Cl_2, deaerated by bubbling a stream of nitrogen through for about 10 minutes, was irradiated with a 420 nm LED for 20 h under stirring, placing the sample at a distance of ca. 3 cm from the light source. Then the solvent was removed under reduced pressure. The yield was estimated from the ^{1}H-NMR analysis using dry dodecane as an internal standard.

Deposition Numbers 2074013 (for **1**), 2074015 (for **2**), and 2074016 (for **3**) contain the supplementary crystallographic data for this paper. These data are provided free of charge by the joint Cambridge Crystallographic Data Centre and Fachinformationszentrum Karlsruhe Access Structures service www.ccdc.cam.ac.uk/structures.

Acknowledgements

Financial support by the DFG-funded transregional collaborative research center SFB/TRR 88 Cooperative Effects in Homo and Heterometallic Complexes (3MET)" is gratefully acknowledged (projects B9, C1 and C7). CB, NSA, TB and C. Bizzarri thank Prof. Bräse for giving access to his laboratories and fruitful discussion. Open access funding enabled and organized by Projekt DEAL.

Conflict of Interest

The authors declare no conflict of interest.

Keywords: ATRA · Cooperativity · Dinuclear Cu(I) Complex · Heteroleptic Cu(I) Complexes · Visible-Light Absorption

[1] N. Armaroli, V. Balzani, *Energy Environ. Sci.* **2011**, *4*, 3193–3222.
[2] a) A. S. Polo, M. K. Itokazu, N. Y. Murakami Iha, *Coord. Chem. Rev.* **2004**, *248*, 1343–1361; b) M. K. Nazeeruddin, M. Grätzel in *Transition Metal Complexes for Photovoltaic and Light Emitting Applications*, (Ed. V. W. W. Yam), Springer Berlin Heidelberg, Berlin, Heidelberg, **2007**, pp. 113–175.
[3] a) C. Bizzarri, E. Spuling, D. M. Knoll, D. Volz, S. Bräse, *Coord. Chem. Rev.* **2018**, *373*, 49–82; b) R. D. Costa, E. Ortí, H. J. Bolink, F. Monti, G. Accorsi, N. Armaroli, *Angew. Chem. Int. Ed.* **2012**, *51*, 8178–8211; *Angew. Chem.* **2012**, *124*, 8300–8334; c) H. Yersin, A. F. Rausch, R. Czerwieniec, T. Hofbeck, T. Fischer, *Coord. Chem. Rev.* **2011**, *255*, 2622–2652.
[4] a) O. S. Wenger, *J. Am. Chem. Soc.* **2018**, *140*, 13522–13533; b) C. B. Larsen, O. S. Wenger, *Chem. Eur. J.* **2018**, *24*, 2039–2058.
[5] a) N. Armaroli, G. Accorsi, F. Cardinali, A. Listorti in *Photochemistry and Photophysics of Coordination Compounds: Copper*, Eds.: V. Balzani and S. Campagna), Springer Berlin Heidelberg, Berlin, Heidelberg, **2007**, pp. 69–115; b) N. Armaroli, *Chem. Soc. Rev.* **2001**, *30*, 113–124.
[6] a) D. R. McMillin, M. T. Buckner, B. T. Ahn, *Inorg. Chem.* **1977**, *16*, 943–945; b) M. W. Blaskie, D. R. McMillin, *Inorg. Chem.* **1980**, *19*, 3519–3522.
[7] L. P. Ravaro, K. P. S. Zanoni, A. S. S. de Camargo, *Energy Rep.* **2020**, *6*, 37–45.
[8] a) M. Sandroni, Y. Pellegrin, F. Odobel, *C. R. Chim.* **2016**, *19*, 79–93; b) M. S. Lazorski, F. N. Castellano, *Polyhedron* **2014**, *82*, 57–70.
[9] a) A. Hossain, A. Bhattacharyya, O. Reiser, *Science* **2019**, *364*, eaav9713; b) Y. Zhang, P. Traber, L. Zedler, S. Kupfer, S. Gräfe, M. Schulz, W. Frey, M. Karnahl, B. Dietzek, *Phys. Chem. Chem. Phys.* **2018**, *20*, 24843–24857; c) S. Paria, O. Reiser, *ChemCatChem* **2014**, *6*, 2477–2483; d) C. Sandoval-Pauker, G. Molina-Aguirre, B. Pinter, *Polyhedron* **2021**, *199*, 115105; e) S. Paria, O. Reiser in *Visible Light and Copper Complexes: A Promising Match in Photoredox Catalysis*, **2018**, pp. 233–251; f) C. Minozzi, A. Caron, J.-C. Grenier-Petel, J. Santandrea, S. K. Collins, *Angew. Chem. Int. Ed.* **2018**, *57*, 5477–5481; *Angew. Chem.* **2018**, *130*, 5575–5579; g) M. F. Greaney, *Science* **2016**, *351*, 666–666; h) Q. M. Kainz, C. D. Matier, A. Bartoszewicz, S. L. Zultanski, J. C. Peters, G. C. Fu, *Science* **2016**, *351*, 681–684; i) S. Oger, H. Baguia, T.-A. Phan, T. Teunens, J. Beaudelot, C. Moucheron, G. Evano, *SynOpen* **2021**, *05*, 141–144; j) B. Michelet, C. Deldaele, S. Kajouj, C. Moucheron, G. Evano, *Org. Lett.* **2017**, *19*, 3576–3579.
[10] S. Garakyaraghi, E. O. Danilov, C. E. McCusker, F. N. Castellano, *J. Phys. Chem. A* **2015**, *119*, 3181–3193.
[11] a) L. L. Gracia, L. Luci, C. Bruschi, L. Sambri, P. Weis, O. Fuhr, C. Bizzarri, *Chem. Eur. J.* **2020**, *26*, 9929–9937; b) C. Bizzarri, A. P. Arndt, S. Kohaut, K. Fink, M. Nieger, *J. Organomet. Chem.* **2018**, *871*, 140–149.
[12] T. M. Williams, C. R. J. Stephenson in *Atom Transfer Radical Addition using Photoredox Catalysis*, **2018**, pp. 73–92.
[13] a) H. Darabi, F. Tahoori, K. Aghapoor, F. Taala, F. Mohsenzadeh, *J. Braz. Chem. Soc.* **2008**, *19*; b) S. Maiti, N. Roy, L. T. Babu, P. Moharana, C. C. Athira, E. Darsana Sreedhar, S. De, S. K. Ashok Kumar, P. Paira, *New J. Chem.* **2020**, *44*, 920–931.
[14] S. Lee, C. Ra, *Clean Technology* **2016**, *22*, 269–273.
[15] F. Himo, T. Lovell, R. Hilgraf, V. V. Rostovtsev, L. Noodleman, K. B. Sharpless, V. V. Fokin, *J. Am. Chem. Soc.* **2005**, *127*, 210–216.
[16] C. Bizzarri, C. Strabler, J. Prock, B. Trettenbrein, M. Ruggenthaler, C.-H. Yang, F. Polo, A. Iordache, P. Brüggeller, L. De Cola, *Inorg. Chem.* **2014**, *53*, 10944–10951.
[17] A. Kaeser, M. Mohankumar, J. Mohanraj, F. Monti, M. Holler, J.-J. Cid, O. Moudam, I. Nierengarten, L. Karmazin-Brelot, C. Duhayon, B. Delavaux-Nicot, N. Armaroli, J.-F. Nierengarten, *Inorg. Chem.* **2013**, *52*, 12140–12151.
[18] a) C. L. Linfoot, P. Richardson, T. E. Hewat, O. Moudam, M. M. Forde, A. Collins, F. White, N. Robertson, *Dalton Trans.* **2010**, *39*, 8945–8956; b) C. Li, W. Li, A. F. Henwood, D. Hall, D. B. Cordes, A. M. Z. Slawin, V. Lemaur, Y. Olivier, I. D. W. Samuel, E. Zysman-Colman, *Inorg. Chem.* **2020**, *59*, 14772–14784; c) L. Lin, D.-H. Chen, R. Yu, X.-L. Chen, W.-J. Zhu, D. Liang, J.-F. Chang, Q. Zhang, C.-Z. Lu, *J. Mater. Chem. C* **2017**, *5*, 4495–4504.
[19] J.-F. Nierengarten, I. Nierengarten, M. Holler, A. Sournia-Saquet, B. Delavaux-Nicot, E. Leoni, F. Monti, N. Armaroli, *Eur. J. Inorg. Chem.* **2019**, *2019*, 2661–2661.
[20] a) K. Saito, T. Arai, N. Takahashi, T. Tsukuda, T. Tsubomura, *Dalton Trans.* **2006**, 4444–4448; b) C. Femoni, S. Muzzioli, A. Palazzi, S. Stagni, S. Zacchini, F. Monti, G. Accorsi, M. Bolognesi, N. Armaroli, M. Massi, G. Valenti, M. Marcaccio, *Dalton Trans.* **2013**, *42*, 997–1010; c) X.-L. Xin, M.

Chen, Y.-b. Ai, F.-l. Yang, X.-L. Li, F. Li, *Inorg. Chem.* **2014**, *53*, 2922–2931; d) A. Listorti, G. Accorsi, Y. Rio, N. Armaroli, O. Moudam, A. Gégout, B. Delavaux-Nicot, M. Holler, J.-F. Nierengarten, *Inorg. Chem.* **2008**, *47*, 6254–6261; e) A. Fazal, A. Al-Dawsari, B. El Ali, L. Ouahab, M. Fettouhi, *J. Coord. Chem.* **2014**, *67*, 2357–2364; f) E. Leoni, J. Mohanraj, M. Holler, M. Mohankumar, I. Nierengarten, F. Monti, A. Sournia-Saquet, B. Delavaux-Nicot, J.-F. Nierengarten, N. Armaroli, *Inorg. Chem.* **2018**, *57*, 15537–15549.

[21] H. A. Jahn, E. Teller, F. G. Donnan, *Proc. R. Soc. London Ser. A* **1937**, *161*, 220–235.

[22] J. Conradie, *Inorg. Chim. Acta* **2019**, *486*, 193–199.

[23] A. Brouwer, *Pure Appl. Chem.* **2011**, *83*, 2213–2228.

[24] H. Ishida, J.-C. Bünzli, A. Beeby, *Pure Appl. Chem.* **2016**, *88*, 701–711.

[25] a) C. Bizzarri, F. Hundemer, J. Busch, S. Bräse, *Polyhedron* **2018**, *140*, 51–66; b) R. Czerwieniec, M. J. Leitl, H. H. H. Homeier, H. Yersin, *Coord. Chem. Rev.* **2016**, *325*, 2–28.

[26] G. Gritzner, J. Kuta, *Pure Appl. Chem.* **1984**, *56*, 461–466.

[27] V. Balzani, P. Ceroni, A. Juris in *Photochemistry and photophysics: concepts, research, applications, Vol.* Wiley-VCH, Weinheim, **2014**.

[28] K. A. Opperman, S. L. Mecklenburg, T. J. Meyer, *Inorg. Chem.* **1994**, *33*, 5295–5301.

[29] S. Jasimuddin, T. Yamada, K. Fukuju, J. Otsuki, K. Sakai, *Chem. Commun.* **2010**, *46*, 8466–8468.

[30] a) S. Paria, M. Pirtsch, V. Kais, O. Reiser, *Synthesis* **2013**, *45*, 2689–2698; b) M. Pirtsch, S. Paria, T. Matsuno, H. Isobe, O. Reiser, *Chem. Eur. J.* **2012**, *18*, 7336–7340; c) O. Reiser, *Acc. Chem. Res.* **2016**, *49*, 1990–1996; d) A. Hossain, S. Engl, E. Lutsker, O. Reiser, *ACS Catal.* **2019**, *9*, 1103–1109; e) D. B. Bagal, G. Kachkovskyi, M. Knorn, T. Rawner, B. M. Bhanage, O. Reiser, *Angew. Chem. Int. Ed.* **2015**, *54*, 6999–7002; *Angew. Chem.* **2015**, *127*, 7105–7108; f) M. M. Cetin, R. T. Hodson, C. R. Hart, D. B. Cordes, M. Findlater, D. J. Casadonte Jr, A. F. Cozzolino, M. F. Mayer, *Dalton Trans.* **2017**, *46*, 6553–6569; g) X.-J. Tang, W. R. Dolbier Jr., *Angew. Chem. Int. Ed.* **2015**, *54*, 4246–4249; *Angew. Chem.* **2015**, *127*, 4320–4323; h) S. Engl, O. Reiser, *ACS Catal.* **2020**, *10*, 9899–9906.

[31] K. Matsuo, E. Yamaguchi, A. Itoh, *Asian J. Org. Chem.* **2018**, *7*, 2435–2438.

[32] A. K. Feldman, B. Colasson, V. V. Fokin, *Org. Lett.* **2004**, *6*, 3897–3899.

[33] F. Furche, R. Ahlrichs, C. Hättig, W. Klopper, M. Sierka, F. Weigend, *Wiley Interdiscip. Rev.: Comput. Mol. Sci.* **2014**, *4*, 91–100.

[34] a) J. P. Perdew, K. Burke, M. Ernzerhof, *Phys. Rev. Lett.* **1996**, *77*, 3865–3868; b) J. P. Perdew, K. Burke, M. Ernzerhof, *Phys. Rev. Lett.* **1997**, *78*, 1396–1396; c) S. Grimme, J. Antony, S. Ehrlich, H. Krieg, *J. Chem. Phys.* **2010**, *132*, 154104; d) S. Grimme, S. Ehrlich, L. Goerigk, *J. Comput. Chem.* **2011**, *32*, 1456–1465.

[35] X. Blase, C. Attaccalite, V. Olevano, *Phys. Rev. B* **2011**, *83*, 115103.

[36] C. Holzer, W. Klopper, *J. Chem. Phys.* **2019**, *150*, 204116.

[37] a) K. Krause, W. Klopper, *J. Comput. Chem.* **2017**, *38*, 383–388; b) X. Gui, C. Holzer, W. Klopper, *J. Chem. Theory Comput.* **2018**, *14*, 2127–2136.

[38] F. Weigend, R. Ahlrichs, *Phys. Chem. Chem. Phys.* **2005**, *7*, 3297–3305.

[39] Y. J. Franzke, R. Treß, T. M. Pazdera, F. Weigend, *Phys. Chem. Chem. Phys.* **2019**, *21*, 16658–16664.

[40] O. V. Dolomanov, L. J. Bourhis, R. J. Gildea, J. A. K. Howard, H. Puschmann, *J. Appl. Crystallogr.* **2009**, *42*, 339–341.

[41] G. Sheldrick, *Acta Crystallogr. Sect. A* **2015**, *71*, 3–8.

[42] G. Sheldrick, *Acta Crystallogr. Sect. C* **2015**, *71*, 3–8.

[43] a) *Chemistry International – Newsmagazine for IUPAC* **2005**, *27*, 25–26; b) E. E. Wegner, A. W. Adamson, *J. Am. Chem. Soc.* **1966**, *88*, 394–404.

Manuscript received: July 27, 2021
Revised manuscript received: August 2, 2021
Accepted manuscript online: August 3, 2021

FULL PAPERS

A broad spectrum of properties for these new heteroleptic Cu(I) complexes shows their versatility in diverse application fields. Their luminescence in solid state reaches a Φ up to 40% at room temperature and they show photoredox activity in a visible-light driven atom transfer radical addition reaction. Furthermore, cooperative effect in the dinuclear complex was observed in electronic absorption and confirmed by theoretical calculations.